



Cite this: DOI: 10.1039/d2sm00218c

## Universal non-Debye low-frequency vibrations in sheared amorphous solids†

Vishnu V. Krishnan, \* Kabir Ramola \* and Smarajit Karmakar \*

We study energy minimised configurations of amorphous solids with a simple shear degree of freedom. We show that the low-frequency regime of the vibrational density of states of structural glass formers is crucially sensitive to the macroscopic stress of the sampled configurations. In both two and three dimensions, shear-stabilised configurations display a  $D(\omega_{\min}) \sim \omega_{\min}^5$  regime, as opposed to the  $\omega_{\min}^4$  regime observed under unstrained conditions. In order to isolate the source of these deviations from crystalline behaviour, we also study configurations of two dimensional, strained amorphous solids close to a plastic event. We show that the minimum eigenvalue distribution at a strain ' $\gamma$ ' near the plastic event occurring at ' $\gamma_p$ ' assumes a universal form that displays a collapse when scaled by  $\sqrt{\gamma_p - \gamma}$ , and with the number of particles as  $N^{-0.22}$ . Notably, at low frequencies, this scaled distribution displays a robust  $D(\omega_{\min}) \sim \omega_{\min}^6$  power-law regime, which survives in the large  $N$  limit. Finally, we probe the properties of these configurations through a characterisation of the second and third eigenvalues of the Hessian matrix near a plastic event.

 Received 12th February 2022,  
 Accepted 4th April 2022

DOI: 10.1039/d2sm00218c

[rsc.li/soft-matter-journal](https://rsc.li/soft-matter-journal)

## 1 Introduction

Amorphous solids are well known to display an anomalous temperature dependence in their heat capacity.<sup>1,2</sup> This has been suggested to originate due to an excess of modes in their vibrational density of states (VDoS), over and above the Debye modes of crystalline systems, and is known as the Boson peak.<sup>3</sup> This behaviour is remarkably robust to the details of the models under consideration, as well as the dimension of the system, and has emerged as a hallmark of amorphous solids. Various theoretical models have been proposed in order to reproduce and characterise this behaviour.<sup>4–11</sup> Since a primary quantity of interest in the thermodynamic limit is the mechanical properties of solid glasses, the relevant scales to probe are their properties at low temperatures, corresponding to low frequencies in the VDoS. Recently, a new vibrational characteristic of glass formers has been identified: a regime displaying a  $D(\omega) \sim \omega^4$  scaling in the density of states.<sup>12–22</sup> Many theoretical models built around two-level systems, replica symmetry breaking, stress correlations, random matrices and other hypotheses have been proposed as the origin of this behaviour,<sup>1,23–33</sup> however, the nature of the modes contributing to the  $\omega^4$  behaviour is still a subject of active research. In this context, it is important to characterise new,

deviant universal features and their connection to microscopic details.

One of the outstanding problems in the field of glass physics is the development of a statistical, microscopic theory explaining their anomalous thermodynamics. Despite considerable theoretical explorations, the best understanding of the glassy regime of matter emerges from simulations. Preparing an athermal, energy minimised ensemble of structural glass-formers allows us to study the statistical properties of rigid configurations that are amorphous in nature. Although assumed to be mechanically stable, such configurations have been shown to contain an additional, strain degree of freedom.<sup>34–37</sup> An otherwise constrained configuration allows for unbalanced shear stresses that may be specific to the simulation parameters.<sup>38</sup> The choice of appropriate states of macroscopic stresses is then an important consideration in the study of amorphous solids.<sup>39,40</sup> While the effect of modulating internal stresses has been studied,<sup>41–43</sup> it is pertinent to re-examine the apparent universality<sup>13,17–19</sup> under physically relevant, macroscopic shear stresses.

In this paper, we study realistic configurations of amorphous solids generated through volume-preserving, simple shear, most notably used in cyclic shearing experiments.<sup>44,45</sup> We use a natural control parameter, namely the simple-shear strain, in order to test the sensitivity of the minimum eigenvalue distributions to specific modifications to the configurations of particles. We show that changes in the macroscopic shear-stress ( $\sigma_{xy}$ ) results in a modification of the amorphous VDoS from  $D(\omega) \sim \omega^4$ , in spite of the internal stress distributions remaining largely invariant. In Section 2, we describe the details of the

Centre for Interdisciplinary Sciences, Tata Institute of Fundamental Research, Hyderabad 500046, India. E-mail: vishnuvk@tifrh.res.in, kramola@tifrh.res.in, smarajit@tifrh.res.in

† Electronic supplementary information (ESI) available. See DOI: <https://doi.org/10.1039/d2sm00218c>

amorphous system we study, and detail the numerical procedures we employ in our explorations. In Section 3 we further examine the measures used to probe vibrational properties. In Section 4 we consider shear-stabilised configurations ( $U = U_{\min}(\gamma)$ ) and show that the low-frequency behaviour of the VDoS shifts to a novel power-law close to  $D(\omega_{\min}) \sim \omega_{\min}^5$ . Such a constraint is relevant to the study of stable solids which, by definition, resist deformations, as examined in Section 5. Additionally, these results point to a link between the  $\omega^4$  regime in the VDoS and the stress fluctuations sustained by the system. In Section 6 we also uncover a new universal distribution of the minimum eigenvalue using configurations at fixed strain-distances to a plastic event. Notably, the distribution collapses under a suitable scaling of the strain as well as the system size. This distribution additionally displays a low-frequency behaviour of  $D(\omega_{\min}) \sim \omega_{\min}^6$ .

## 2 Methods and simulation details

### 2.1 Simulation potentials

We simulate a 50 : 50 mixture of two particle types A and B. The interaction potentials are cut-off at a distance

$$r_c = 1.385418025\sigma, \quad (1)$$

with the three interaction diameters given by

$$\begin{aligned} \sigma_{AA} &= 1.0, \\ \sigma_{BB} &= 1.4, \\ \sigma_{AB} &= \sqrt{\sigma_{AA}\sigma_{BB}}. \end{aligned} \quad (2)$$

The only difference between the parameters in two and three dimensions of this model are the reduced number densities given by

$$\begin{aligned} \rho_{2D} &= 0.85, \\ r_{3D} &= 0.81. \end{aligned} \quad (3)$$

In our simulations we focus on the purely repulsive pairwise potential, given by a tenth order polynomial, termed 'R10'. The potential smooth to  $n$  derivatives at cut-off is given by

$$\psi = \left(\frac{\sigma}{r}\right)^{10} + \sum_{m=0}^n c_{2m} \left(\frac{r}{\sigma}\right)^{2m} \quad (4)$$

where the constants are calculated appropriately. We use only even-powered polynomials in order to avoid the potential curving downwards at the cut-off, to any precision, thus eliminating any attraction at the cut-off.

### 2.2 Sample sizes

Tables 1 and 2.

### 2.3 Software

Simulations of glasses along with the energy minimizations were performed using LAMMPS.<sup>61,62</sup> The stopping criterion for the minimization was the force 2-norm:  $\sqrt{\sum_{i=1}^N |F_i|^2}$ . Eigenvalue

**Table 1** Number of minimum eigenvalue samples collected toward binning the  $P(\lambda_{\min})$  histograms plotted in Fig. 3 and Fig. S4 in the ESI, with the suffix 'k' indicating a thousand

Dimension	2		3	
System size ( $N$ )	256	1024	4096	512
Samples	256k	256k	150k	256k

**Table 2** Number of minimum eigenvalue samples collected toward binning the plastic-event approach  $P(\lambda_{\min,2,3})$  histograms plotted in Fig. 5 and 6 in the main text and in Fig. S5 in the ESI, with the suffix 'k' indicating a thousand

Dimension	2		
System size ( $N$ )	256	1024	4096
Samples	256k	50k	50k

calculations were performed using the LAPACK<sup>63</sup> routine dsyevr for small systems, and the Intel MKL<sup>64</sup> sparse solver routine mkl\_sparse\_d\_ev for large-sized matrices. Analyses were performed using NumPy<sup>65-67</sup> and SciPy<sup>68,69</sup> libraries. Plotting was performed using Matplotlib.<sup>70,71</sup>

### 2.4 Athermal configurations

**2.4.1 Unstrained.** In our simulations, we use two-dimensional glass formers with varying particle numbers  $N \in \{256, 1024, 4096\}$  and a three-dimensional system of size  $N = 512$ , equilibrated at a parent temperature  $T_p = 0.58$ , and then cool to near-zero temperature at a slow rate of  $\dot{T} \approx 10^{-2}$ . We then employ the conjugate gradient algorithm to achieve an energy minimised state up to a force tolerance of  $1.0 \times 10^{-10}$ . These comprise the Unstrained configurations. We also use these to generate the shear-stabilised configurations.

**2.4.2 Zero-shear-stress.** We begin with an Unstrained configuration and calculate the total shear stress ( $\sigma_{xy}$ ). We then strain the configuration in the direction of the stress. For example, if the shear stress is negative, then the system is strained towards the left. This choice of the straining direction is determined by the direction of the initial stress in each configuration. This causes the stress to decrease in magnitude, and we proceed until the stress reverses direction. We perform the same operation two more times, each time with decreasing strain increments. The three strain steps we use are:  $\Delta\gamma \in \{5 \times 10^{-5}, 10^{-8}, 10^{-11}\}$ . The eigenvalues typically were not seen to vary much beyond the first strain step, but we proceed to ensure that we are not separated from the shear-stabilised state by a plastic event. When performing athermal quasi-static shearing (AQS), we use Lees-Edwards boundary conditions and strain at an engineering strain rate of  $5.0 \times 10^{-5}$ . At every step, the structure is relaxed to its minimum energy, to a force tolerance of  $1.0 \times 10^{-10}$ .

**2.4.3 Shear-strain-energy-minimised.** The configurations were generated using the LAMMPS procedure box/relax. The primary utility of this algorithm is that it allows one to perform

energy minimisations allowing the shape of the simulation box to change, while also maintaining periodic boundaries. We make use of the procedure with only the shear-strain included as a degree of freedom aside from the particle positions. As highlighted in the documentation,<sup>62</sup> this method encounters issues due to the algorithm utilising the initial, unstrained box dimensions as a reference for the stress computation. The effect of this is that configurations that are at a large strain away from a stable state and those configurations that suffer plastic events before attaining shear-stability both fail to achieve minimisation to the desired force tolerance. This is remedied, as suggested in the documentation, in two ways: first by utilising the nreset option to recalculate the reference box dimensions and second by restarting the minimiser upon failure, typically across plastic events.

**2.4.4 Plastic-event-approach.** Plastic events are said to have occurred when there are non-affine displacements with a localised spatial extent and a small fraction of participating particles. These displacements differ from the typical elastic, affine response of the particles to the applied strain, most significantly in that the total magnitude of the displacement is much larger. An important feature of these events is the quadrupolar nature of the displacement field, centred at the point of localisation, signalling a T1-like event. In order to ‘detect’ a plastic event, we utilise a convenience of the AQS protocol, being that every step of straining involves two stages: (a) application of an affine strain and (b) an energy minimisation. Plastic events present large displacements in stage (b) of the protocol. Therefore, we keep track of the displacement of the maximally displaced particle at every step of energy minimisation and register a plastic event when that value crosses a threshold. For our model, we use a value of  $\approx 15 \times \delta\gamma$ , whereas under elastic conditions the maximum displacements during minimisation are  $\sim \delta\gamma$ . The value of the displacement cut-off is chosen so as to obtain localised, quadrupolar events and avoid other non-affine relaxations. Additionally, in order to avoid some corner-case scenarios, we also utilise a minimum energy threshold of  $10^{-9}$  energy units for a step to register as a plastic event at a particular strain ( $\gamma_p$ ).

Given such a mechanism to detect plastic events, we now define an ensemble of configurations that all need the same ‘strain’ to incur a plastic event ( $\Delta\gamma = \gamma_p - \gamma$ ). The procedure we follow is that, for each configuration ‘ $i$ ’, we find its plastic strain  $\gamma_p^i$ , and then we strain each configuration to a corresponding strain ‘ $\gamma^i$ ’ such that all the configurations are at the same distance-in-strain away from their respective plastic events,  $\gamma_p^i - \gamma^i = \Delta\gamma$ . Note that  $\Delta\gamma > 0$ . In order to sample small enough values of  $\Delta\gamma$ , we first measure the plastic-strain,  $\gamma_p$ , to an accuracy of  $10^{-8}$  by ‘back-tracking’ to a previous state upon encountering a plastic-event, and subsequently straining the system at the requisite precision. Thus, we are able to sample configurations of the system at various values of the strain-to-plastic-event:  $\Delta\gamma \in \{10^{-3}, 10^{-4}, 10^{-5}, 10^{-6}, 10^{-7}\}$ .

### 3 Minimum eigenvalue spectrum

The vibrational properties of a solid may be discerned from the Hessian of the total potential energy  $U[\{\mathbf{r}^i\}] = \sum_{ij} \psi^{ij}$ , where  $\psi^{ij}$

is the interaction potential between particles  $i$  and  $j$  which we assume to be central. This is conveniently represented by the Hessian matrix

$$\mathcal{H}_{\alpha\beta}^{ij}(\mathbf{r}^{ij}) = \frac{\partial^2 U[\{\mathbf{r}^i\}]}{\partial r_\alpha^i \partial r_\beta^j}, \quad (5)$$

the indexes of which run over dimensions  $\alpha, \beta \in \{x, y, z\}$  for every pair of particles  $i, j \in \{1, \dots, N\}$ . Above,  $r_\alpha^i$  is the  $\alpha$ -component of the distance vector from particle  $i$  to  $j$ . A primary quantity of interest in the study of the vibrational properties of glasses is the distribution of the minimum eigenvalue of the Hessian matrix,  $\lambda_{\min}$ . This typically controls the longest time scales in the system and provides a useful route to characterise the stability of amorphous solids.<sup>46</sup>

The vibrational frequencies are related to the eigenvalue of the Hessian as  $\omega = \sqrt{\lambda}$ . This allows us to relate the two distributions as  $D(\omega) = \sqrt{\lambda}P(\lambda)$ . However, since we are interested in the low-frequency regime of the VDoS, we measure the distribution of the minimum eigenvalue of the Hessian. Moreover, in the case of independent and identically distributed random variables, power-laws at the tails are reproduced by an extreme value sampling, *i.e.*,  $P(x) \sim x^\alpha$  implies that  $P(x_{\min}) \sim x_{\min}^\alpha$ . Additionally, by only calculating the minimum eigenvalue, we are able to achieve the large numbers of samples necessary to observe localised modes. Many glass formers display a  $P(\lambda_{\min}) \sim \lambda_{\min}^{1.5} \equiv D(\omega_{\min}) \sim \omega_{\min}^4$  behaviour in the tail of the minimum eigenvalue distribution, indicating weak correlations in the low lying eigenvalues.<sup>12</sup> Deviations from this universal behaviour are therefore of interest in determining different structural properties of glasses. Indeed, we show in this Letter that the response of short ranged glass formers to shear is linked to changes in  $P(\lambda_{\min})$ , which in turn is crucially sensitive to the macroscopic stresses of the configurations.

### 4 Shear-stabilised configurations

We consider configurations that are allowed to undergo volume-preserving, simple shear, where only the upper-triangular elements of the strain tensor can be non-zero ( $\gamma_{\alpha\beta} = \varepsilon_{\alpha\beta}^{\alpha < \beta}$ ). An isolated stable solid relaxes along all available degrees of freedom. In such energy minimised configurations of systems comprising particles interacting *via* pairwise, central potentials, the off-diagonal element of the macroscopic force moment tensor, *i.e.*, the shear stress is exactly zero,<sup>47</sup> as illustrated in Fig. 1:

$$\frac{\partial U}{\partial \gamma_{\alpha\beta}} = \sum_{(i,j)} f_\alpha^{ij} r_\beta^{ij} = \sum_{(i,j)} \sigma_{\alpha\beta}^{ij} \equiv \sigma_{\alpha\beta} \times V, \quad (6)$$

where  $f_\alpha^{ij}$  is the  $\alpha$ -component of the force on particle  $i$  by particle  $j$ ,  $\sigma_{\alpha\beta}^{ij}$  is the bond-stress between particles  $i$  and  $j$ ,  $\sigma_{\alpha\beta}$  is the macroscopic stress tensor and  $V$  is the volume of the system. It is therefore natural to probe the effect of macroscopic shear stress fluctuations on the stability properties of such systems, which are enhanced due to relaxation along an additional strain degree of freedom.

In this context, we analyse the distribution of minimum eigenvalues of the Hessian matrices of configurations sampled

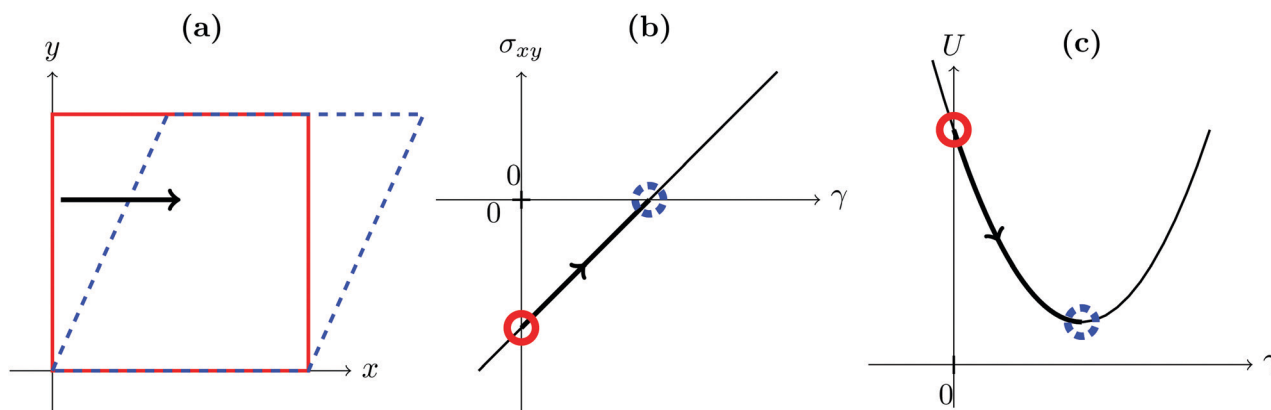


**Fig. 1** (a) Schematic representation of a system undergoing simple shear and the corresponding changes in (b) stress and (c) energy. The (red) solid state represents an unstrained state that exhibits a finite shear-stress. The (blue) dashed state represents a shear-stabilised state.

from two sets of configurations with (i) finite shear stress fluctuations and (ii) zero shear stress fluctuations (within a tolerance). Configurations with finite stresses appear naturally when generating energy minimised configurations from a thermal ensemble, under periodic boundary conditions, as maybe shown in Fig. 2, and we refer to these as Unstrained configurations. We create shear-stabilised configurations using two different procedures. In the first method, we athermally strain the system in the direction of the shear stress until the stress changes sign, and this is repeated two more times, with reduced strain increments. We term these configurations zero-shear-stress (Section A of the ESI†<sup>48</sup> shows the strains required). Such a procedure allows us to attain stress-free states in systems with one shear-stress, namely, systems in two dimensions. Therefore, we also use a

technique capable of relaxing stresses in three dimensional systems. In the second method, we perform an energy minimisation of the position as well as shear strain degrees of freedom concomitantly, and refer to these configurations as shear-strain-energy-minimised. Notably, these protocols leave the statistics of the internal bond-stresses invariant (see Section B of the ESI†<sup>48</sup>).

We display numerically sampled minimum eigenvalue distributions of the Hessian for two (2D) and three dimensional (3D) systems in Fig. 3. Remarkably, the minimum eigenvalue distributions corresponding to the two types of configurations yield markedly different results, especially at the lowest frequencies which govern large-scale stability properties. Specifically, we find that the well-known  $\omega_{\min}^4$  regime is modified

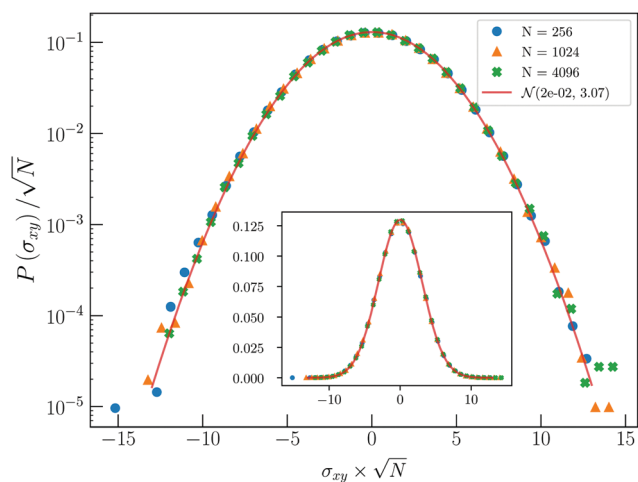


**Fig. 2** Stress distributions of configurations generated by cooling and energy-minimising a thermal ensemble under periodic boundaries. The plot shows the stress fluctuations of system sizes  $N \in \{256, 1024, 4096\}$ . The distributions scale with system size as  $1/\sqrt{N}$  in two dimensions. The solid line is a maximum-likelihood-estimate fit of the normal distribution to the data corresponding to  $N = 4096$ , with fit parameters shown in the legend. These plots quantify the effective residual stresses present in simulated models of amorphous solids when prepared under unstrained conditions. A log-linear scale is used, while the inset is plotted in a linear-linear scale.

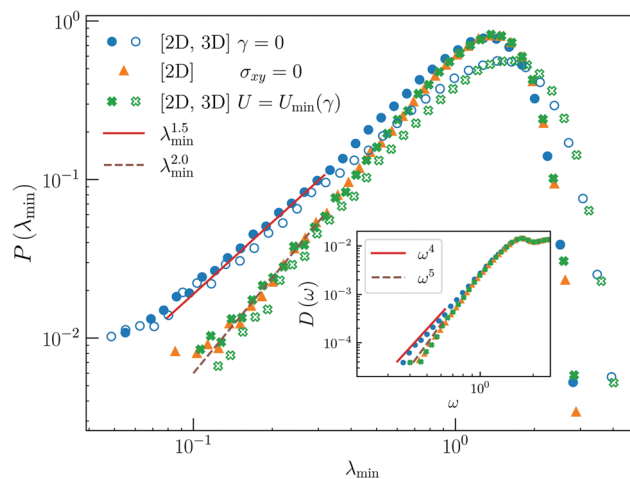


**Fig. 3** Minimum eigenvalue distributions obtained from energy minimised configurations of a 2D system of 256 particles. The unfilled markers correspond to a 3D system of 512 particles. The plots compare typical Unstrained configurations (blue circles) against the shear-stabilised configurations: zero-shear-stress (orange triangles) and shear-strain-energy-minimised (green crosses). The distributions drawn from these configurations deviate significantly from the  $\omega_{\min}^4$  regime. The (red) solid and (violet) dashed lines correspond to power-laws of  $\omega_{\min}^4$  and  $\omega_{\min}^5$ , respectively. (inset) Distribution of the full vibrational density of states for a 2D system with 256 particles. The low frequency behaviour of the distribution is modified from  $D(\omega) \sim \omega^4$  to  $D(\omega) \sim \omega^5$ .

in the shear-stabilised configurations, and instead we find the best-fit power-law to be closer to  $\omega_{\min}^5$ . For data on larger system sizes, see Section C of the ESI.†<sup>48</sup> Moreover, we find that the two different procedures of generating a shear-stabilised configuration yield identical distributions, pointing to the fact that these distributions are sensitive to the stress ensemble and not the preparation protocol, independent of the dimension.

## 5 Mechanical properties

Understanding the relationship between microscopic parameters and bulk rigidity is important in constructing a first-principles theory of solids. In order to further probe the connection between the minimum eigenvalue distributions and the stability of configurations created in the different states of stress, we carry out athermal quasistatic shearing (AQS) of the system,<sup>49</sup> using 2D glass structures. AQS allows us to trace the state of a local minimum as the potential energy surface is transformed under an effectively infinitesimal strain rate. Amorphous materials as well as crystals, when subjected to an incremental strain, produce a corresponding linear stress-response. However, unlike crystals, amorphous arrangements of particles incur localised, non-affine, displacements termed ‘plastic events’. These deformations are easily identified in an athermal straining protocol by the occurrence of abrupt stress-drops and localised particle displacements. The amorphous nature of the constituent particles allows the system to release stresses *via* such events that comprise displacements of a small fraction of the particles that occur when energy-minimising the system after subjecting it to an affine strain.

The distribution of the strain needed to induce the first plastic event forms an important descriptor of the rigidity of solids and is an indicator of their stability to shear. It is therefore important to study the nature of such distributions using configurations that display experimentally relevant stresses. As discussed in eqn (6), the shear-stabilised configurations with zero shear stress may provide an accurate characterisation of the stability of real solids. In Fig. 4 we show that the distribution of the strain  $\Delta\gamma_1$  needed to achieve the first plastic event is sensitive to the stress-fluctuations allowed in the configurations sampled. Most significantly, unstrained configurations are more susceptible to plastic events at lower strain-deformations. Intriguingly, the estimated exponent ( $P(\Delta\gamma_1) \sim \Delta\gamma_1^\theta$ ) in the low  $\Delta\gamma_1$  regime, an important characterisation of amorphous stability,<sup>50,51</sup> seems to increase from  $\theta \approx 0.4$  to  $\theta \approx 0.45$  between the unstrained and shear-stabilised configurations.

## 6 Configurations approaching a plastic-event

Since a primary utility of a Hessian analysis is the determination of the stability of amorphous systems, it is natural to focus on the nature of configurations of near-failure amorphous solids. These plastic events correspond to the system crossing saddles in the energy landscape as it is sheared.<sup>52</sup> Traversing across such

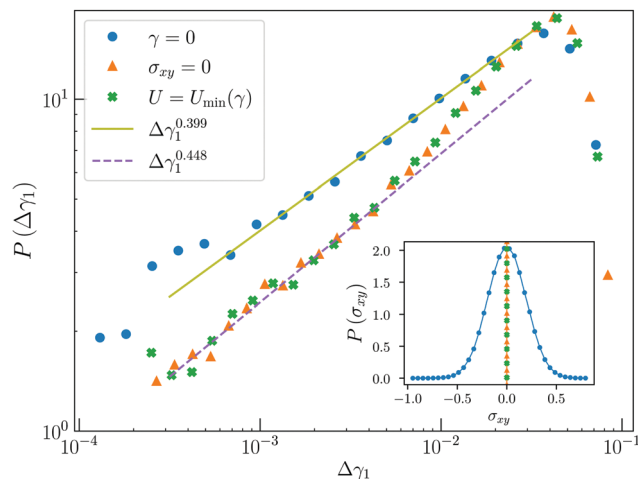


Fig. 4 Distributions of the strain  $\Delta\gamma_1$  required to achieve the first plastic event, beginning with configurations sampled from the Unstrained and from the two shear-stabilised configurations. These measurements were performed on 2D systems of size  $N = 256$  in two dimensions. The lines indicate best-fits for the exponent. The shear-stabilised configurations have fewer plastic events at smaller strains. (inset) Distribution of the macroscopic shear stress in energy minimised configurations. The unstrained configurations display finite shear-stress fluctuations, while the shear-stabilised configurations possess no macroscopic shear stress.

energy barriers by straining the system allows us to probe the energy landscape that determines the stability of such amorphous configurations of particles. The model system used allows us to study its properties close to such a phenomenon. Once the plastic event is identified, as described in the previous section, we then proceed to ascertain the strain  $\gamma_p$ , at which the plastic event occurs, to a high degree of precision by using very fine strain-steps. This permits us to sample configurations that are arbitrarily close to the event. We thus define the collection of plastic-event-approach configurations that are all at the same strain to their respective plastic events ( $\Delta\gamma = \gamma_p - \gamma$ ).

We study the single most important marker of stability, namely the minimum eigenvalue of the Hessian, as the system approaches the plastic-strain ( $\gamma_p$ ) at which a saddle in the energy landscape is reached. The behaviour of the displacement field has been shown to be proportional to the minimum eigenmode, when close to such a plastic event:<sup>53</sup>

$$\mathbf{u}(\gamma) - \mathbf{u}(\gamma_p) = X(\gamma)\psi_{\min}, \quad (7)$$

where  $\mathbf{u}$  represents the position of the particles as a function of the strain  $\gamma$  and  $X$  is the projection of the displacement field onto the minimum eigenvector  $\psi_{\min}$ . The minimum eigenvalue is assumed to vary linearly with the projection  $\lambda_{\min} \approx \alpha X(\gamma)$ , which in turn leads to an approach to zero with a square-root singularity:  $\lambda_{\min} \approx \alpha\sqrt{\gamma_p - \gamma}$ . This singular behaviour occurs due to the eigenvector corresponding to the minimum eigenvalue aligning itself with the displacement vector corresponding to the plastic event. A natural question then is the exact nature of the proportionality constant  $\alpha$  that governs the magnitude of the change in the minimum eigenvalue of the Hessian with the strain of the system. The singular square-root approach is quite

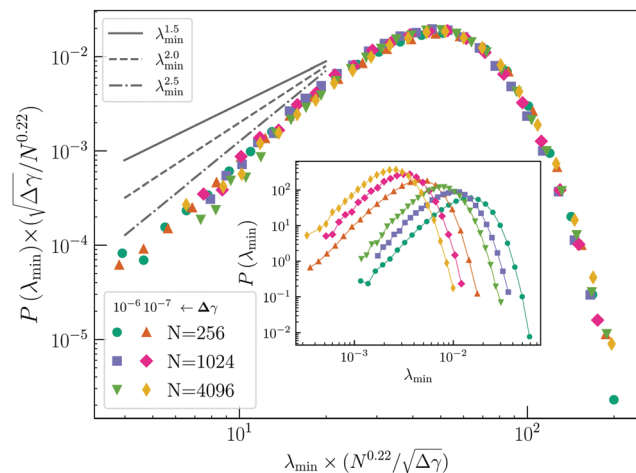


**Fig. 5** Distributions of the minimum eigenvalue of the Hessian matrix,  $\lambda_{\min}$ , drawn from strained configurations grouped by distance  $\Delta\gamma$  from their respective first plastic events (inset). These distributions collapse when scaled by the strain gap as  $\sqrt{\Delta\gamma}$  and the number of particles as  $N^{-0.22}$ . These scaled distributions show a marked deviation from  $\omega_{\min}^4$  behaviour (solid line). The dash-dotted line corresponds to a power-law of  $\omega_{\min}^6$ .

general and is expected whenever a system approaches a saddle corresponding to a plastic event along one of its degrees of freedom. For example, a crystalline system undergoing a slip will have its eigenvalue vanish with a single  $\alpha$  determined by the interactions between the particles. On the other hand, amorphous materials differ in that the constant of proportionality  $\alpha$  varies from sample to sample. The statistics of  $\alpha$  is consequently dependent purely on the microscopic parameters of the system, and we therefore expect a universal distribution of the form:

$$P(\alpha) \equiv P\left(\frac{\lambda_{\min}}{\sqrt{\gamma_P - \gamma}}\right). \quad (8)$$

In Fig. 5, we display these distributions at small distances to the plastic strain as well as for various system sizes. We scale these distributions with the strain-distance as  $\sqrt{\Delta\gamma}$  and system size as approximately  $N^{-0.22}$ . This universal distribution seems to exhibit a low-frequency power-law of  $\lambda_{\min}^{2.5}$  corresponding to  $\omega_{\min}^6$ . The full approach to the plastic event is illustrated in Section D of the ESI.<sup>†</sup><sup>48</sup> Attempts at fitting one of the three common extreme value distributions failed to yield a reasonable match, suggesting a non-trivial limiting form. Using the estimated exponent  $\alpha \approx 2.5$  in an extreme value fit of uncorrelated variables predicts a scaling with  $N$  with an exponent  $1/(1 + \alpha) \approx 0.286$ . The significant difference from our observed system size scaling exponent of 0.22 also points to correlations in the underlying eigenvalues, which would be interesting to characterise further.

### 6.1 Second and third eigenvalue distributions

The Hessian matrices of amorphous systems have also been sought to be modelled within random matrix frameworks.<sup>26,54–58</sup> In this context, we analyse the behaviour of the second and third eigenvalues  $\lambda_2$  and  $\lambda_3$ , as the system approaches a plastic event. Notably, in the limit of a vanishing minimum eigenvalue, the second eigenvalue is equivalent to the first level-spacing. Such

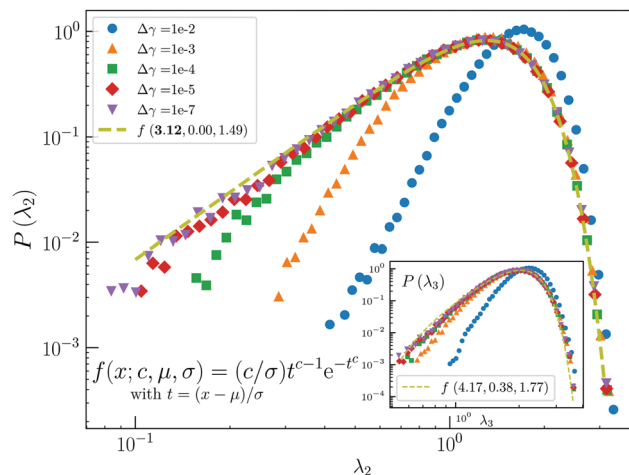


**Fig. 6** Distributions of the second eigenvalue of  $N = 256$  systems, as it approaches the plastic event. Surprisingly, the distribution approaches a Weibull form as the plastic event is approached. The dashed line is a two-parameter Weibull fit with  $\mu$  set to 0. (inset) Distribution of the third eigenvalue in the same system. This distribution does not fit well to a generalised extreme value form. The best fit is displayed by the dashed line.

near-extreme value distributions are natural measures that arise in random matrix theory,<sup>59,60</sup> and could therefore serve as useful tools to understand the nature of the ensemble that the Hessian matrices of amorphous solids generate.

As the plastic event is approached, the minimum eigenvalue departs from the remaining vibrational frequencies. The effect of such a separation is clearly felt by the remnant of the spectrum, as can be seen in Fig. 6. Interestingly, as the system approaches this saddle point, the distribution of the second eigenvalue converges to a zero-located Weibull distribution. Such Weibull forms have also been observed in the minimum eigenvalue distributions in glass formers for small system sizes.<sup>12</sup> Our best fit curve is displayed in Fig. 6, showing a very good match. Additionally, the fit estimates a low-frequency power-law of about  $\lambda_2^{2.12}$ . Such a characterisation assumes relevance when studying solids close to plastic events because the VDoS may then be well represented by a spectrum with one less mode than otherwise. Finally we also measure the statistics of the third eigenvalue as the plastic event is approached. We plot this distribution in the inset of Fig. 6. Once again, this distribution attains a limiting form. However, this distribution does not seem to fit well with the generalised extreme value distributions.

## 7 Conclusions

We have presented results highlighting the role played by the choice of configurations in the low-frequency regime of the VDoS of structural glass formers. We find that crucially finite shear stress fluctuations are required to observe the universal  $\omega_{\min}^4$  regime that has emerged as a hallmark of low-temperature glasses. Determining the appropriate distributions of stresses in real amorphous solids prepared under different conditions

and their effect on structural properties would therefore be of immediate relevance. We also showed that the minimum eigenvalue of the Hessian attains a universal distribution when approaching a plastic event. It would be interesting to probe the origin of the anomalous scaling of  $N^{-0.22}$  with the number of particles displayed by this distribution. The robustness of the  $\omega_{\min}^4$  regime in the VDoS of amorphous solids in the context of our study motivates an analysis of different models of structural glass formers in stress-controlled ensembles, in two as well as three dimensions. Similarly, studying the effects of varying the smoothness in the interaction potentials which have been shown to have non-trivial effects on the Hessian matrices<sup>72</sup> could help better understand the stability of amorphous solids to shear. Finally, it would also be interesting to study the shear stress fluctuations in ultrastable glasses, which have been shown to have anomalous rigidity properties.<sup>73</sup>

## Conflicts of interest

There are no conflicts to declare.

## Acknowledgements

We thank Edan Lerner, Jishnu Nampoothiri and Srikanth Sastry for useful discussions. V. V. K. thanks the Council of Scientific and Industrial Research, India for support *via* the Shyama Prasad Mukherjee Fellowship (SPM-07/1142(0228)/2015-EMR-1). S. K. would like to acknowledge the support *via* Swarna Jayanti Fellowship Grant No. DST/SJF/PSA-01/2018-19 and SB/SFJ/2019-20/05. This project was funded by intramural funds at TIFR Hyderabad from the Department of Atomic Energy, Government of India.

## Notes and references

- U. Buchenau, Y. M. Galperin, V. L. Gurevich and H. R. Schober, *Phys. Rev. B*, 1991, **43**, 5039–5045.
- M. A. Ramos, *Philos. Mag.*, 2004, **84**, 1313–1321.
- U. Buchenau, N. Nücker and A. J. Dianoux, *Phys. Rev. Lett.*, 1984, **53**, 2316–2319.
- P. W. Anderson, B. I. Halperin and C. M. Varma, *Philos. Mag.*, 1972, **25**, 1–9.
- W. A. Phillips, *J. Low Temp. Phys.*, 1972, **7**, 351–360.
- U. Buchenau, A. Wischnewski, M. Ohl and E. Fabiani, *J. Phys.: Condensed Matter*, 2007, **19**, 205106.
- M. Baggioli and A. Zaccane, *Phys. Rev. Lett.*, 2019, **122**, 145501.
- A. Zaccane, *J. Phys.: Condens. Matter*, 2020, **32**, 203001.
- M. Baggioli and A. Zaccane, *Phys. Rev. Res.*, 2020, **2**, 013267.
- L. Casella, M. Baggioli, T. Mori and A. Zaccane, *J. Chem. Phys.*, 2021, **154**, 014501.
- M. Baggioli and A. Zaccane, *Int. J. Mod. Phys. B*, 2021, **35**, 2130002.
- E. Lerner, G. Düring and E. Bouchbinder, *Phys. Rev. Lett.*, 2016, **117**, 035501.
- G. Kapteijns, E. Bouchbinder and E. Lerner, *Phys. Rev. Lett.*, 2018, **121**, 055501.
- M. Paoluzzi, L. Angelani, G. Parisi and G. Ruocco, *Phys. Rev. Lett.*, 2019, **123**, 155502.
- L. Wang, A. Ninarello, P. Guan, L. Berthier, G. Szamel and E. Flenner, *Nat. Commun.*, 2019, **10**, 1–7.
- F. Arceri and E. I. Corwin, *Phys. Rev. Lett.*, 2020, **124**, 238002.
- D. Richard, K. González-López, G. Kapteijns, R. Pater, T. Vaknin, E. Bouchbinder and E. Lerner, *Phys. Rev. Lett.*, 2020, **125**, 085502.
- S. Bonfanti, R. Guerra, C. Mondal, I. Procaccia and S. Zapperi, *Phys. Rev. Lett.*, 2020, **125**, 085501.
- M. Shimada, H. Mizuno, L. Berthier and A. Ikeda, *Phys. Rev. E*, 2020, **101**, 052906.
- P. Das, H. G. E. Hentschel, E. Lerner and I. Procaccia, *Phys. Rev. B*, 2020, **102**, 014202.
- M. Paoluzzi, L. Angelani, G. Parisi and G. Ruocco, *Phys. Rev. Res.*, 2020, **2**, 043248.
- P. Das and I. Procaccia, *Phys. Rev. Lett.*, 2021, **126**, 085502.
- V. L. Gurevich, D. A. Parshin and H. R. Schober, *Phys. Rev. B*, 2003, **67**, 094203.
- V. Gurarie and J. T. Chalker, *Phys. Rev. B*, 2003, **68**, 134207.
- D. A. Parshin, H. R. Schober and V. L. Gurevich, *Phys. Rev. B*, 2007, **76**, 064206.
- E. Stanifer, P. K. Morse, A. A. Middleton and M. L. Manning, *Phys. Rev. E*, 2018, **98**, 042908.
- H. Ikeda, *Phys. Rev. E*, 2019, **99**, 050901(R).
- B. Cui and A. Zaccane, *Eur. Phys. J. E*, 2020, **43**, 1–7.
- E. Bouchbinder, E. Lerner, C. Rainone, P. Urbani and F. Zamponi, *Low-frequency vibrational spectrum of mean-field disordered systems*, 2021.
- M. Shimada, H. Mizuno and A. Ikeda, *Soft Matter*, 2021, **17**, 346–364.
- M. Shimada, H. Mizuno and A. Ikeda, *Soft Matter*, 2020, **16**, 7279–7288.
- D. A. Conyuh and Y. M. Beltukov, *Phys. Rev. B*, 2021, **103**, 104204.
- C. Rainone, P. Urbani, F. Zamponi, E. Lerner and E. Bouchbinder, *SciPost Phys. Core*, 2021, **4**, 8.
- S. Dagois-Bohy, B. P. Tighe, J. Simon, S. Henkes and M. van Hecke, *Phys. Rev. Lett.*, 2012, **109**, 095703.
- Y. Wu, P. Olsson and S. Teitel, *Phys. Rev. E*, 2015, **92**, 052206.
- Y. Wu and S. Teitel, *Phys. Rev. E*, 2015, **91**, 022207.
- Y. Wu and S. Teitel, *Phys. Rev. E*, 2015, **92**, 022207.
- Periodic boundary conditions together with the preparation protocols generate configurations corresponding to a non-zero shear stress ensemble due to constrained rotational freedom.
- S. Henkes and B. Chakraborty, *Phys. Rev. E*, 2009, **79**, 061301.
- D. Bi, J. Zhang, R. Behringer and B. Chakraborty, *Europhys. Lett.*, 2013, **102**, 34002.
- H. Mizuno, H. Shiba and A. Ikeda, *Proc. Natl. Acad. Sci. U. S. A.*, 2017, **114**, E9767–E9774.
- E. Lerner and E. Bouchbinder, *Phys. Rev. E*, 2018, **97**, 032140.

- 43 A. Moriel, *Phys. Rev. Lett.*, 2021, **126**, 088004.
- 44 N. C. Keim, J. Hass, B. Kroger and D. Wieker, *Phys. Rev. Res.*, 2020, **2**, 012004.
- 45 E. G. Teich, K. L. Galloway, P. E. Arratia and D. S. Bassett, *Sci. Adv.*, 2021, **7**, eabe3392.
- 46 C. Maloney and A. Lematre, *Phys. Rev. Lett.*, 2004, **93**, 195501.
- 47 S. Karmakar, E. Lerner and I. Procaccia, *Athermal nonlinear elastic constants of amorphous solids*, 2010, Appendix C.
- 48 See the ESI† for details.
- 49 S. Kobayashi, K. Maeda and S. Takeuchi, *Acta Metall.*, 1980, **28**, 1641–1652.
- 50 J. Lin, A. Saade, E. Lerner, A. Rosso and M. Wyart, *EPL (Europhysics Letters)*, 2014, **105**, 26003.
- 51 J. Lin, E. Lerner, A. Rosso and M. Wyart, *Proc. Nat. Acad. Sci. U. S. A.*, 2014, **111**, 14382–14387.
- 52 C. E. Maloney and A. Lematre, *Phys. Rev. E*, 2006, **74**, 016118.
- 53 S. Karmakar, A. Lematre, E. Lerner and I. Procaccia, *Phys. Rev. Lett.*, 2010, **104**, 215502.
- 54 Y. M. Beltukov and D. A. Parshin, *Phys. Solid State*, 2011, **53**, 151–162.
- 55 Y. M. Beltukov, V. I. Kozub and D. A. Parshin, *Phys. Rev. B*, 2013, **87**, 134203.
- 56 M. L. Manning and A. J. Liu, *Europhys. Lett.*, 2015, **109**, 36002.
- 57 D. A. Conyuh, Y. M. Beltukov and D. A. Parshin, *J. Phys.: Conf. Ser.*, 2017, **929**, 012031.
- 58 M. Baggioli, R. Milkus and A. Zaccone, *Phys. Rev. E*, 2019, **100**, 062131.
- 59 M. L. Mehta, *Random Matrices and the Statistical Theory of Energy Levels*, Elsevier, New York, 2014.
- 60 C. E. Porter, *Statistical Theories of Spectra: Fluctuations*, Academic Press, 1965.
- 61 S. Plimpton, *J. Comput. Phys.*, 1995, **117**, 1–19.
- 62 Large-scale Atomic/Molecular Massively Parallel Simulator, Sandia National Laboratories, 2003, Versions: 5 Jun 2019, 3 March 2020.
- 63 E. Anderson, Z. Bai, C. Bischof, S. Blackford, J. Demmel, J. Dongarra, J. Du Croz, A. Greenbaum, S. Hammarling, A. McKenney and D. Sorensen, *LAPACK Users' Guide*, Society for Industrial and Applied Mathematics, Philadelphia, PA, 3rd edn, 1999.
- 64 Intel, Math Kernel Library, 2019.
- 65 S. van der Walt, S. C. Colbert and G. Varoquaux, *Comput. Sci. Eng.*, 2011, **13**, 22–30.
- 66 C. R. Harris, K. J. Millman, S. J. van der Walt, R. Gommers, P. Virtanen, D. Cournapeau, E. Wieser, J. Taylor, S. Berg and N. J. Smith, *et al.*, *Nature*, 2020, **585**, 357–362.
- 67 NumPy, Version: 1.20.1, 2021.
- 68 P. Virtanen, R. Gommers and T. E. Oliphant, *et al.*, *Nat. Methods*, 2020, **17**, 261–272.
- 69 SciPy, Version: 1.6.2, 2021.
- 70 J. D. Hunter, *Comput. Sci. Eng.*, 2007, **9**, 90–95.
- 71 Matplotlib, Version: 3.4.1, 2021.
- 72 V. V. Krishnan, S. Karmakar and K. Ramola, *Phys. Rev. Res.*, 2020, **2**, 042025(R).
- 73 M. Ozawa, L. Berthier, G. Biroli, A. Rosso and G. Tarjus, *Proc. Nat. Acad. Sci. U. S. A.*, 2018, **115**, 6656–6661.